



Boumediri, H., Bezazi, A., Del Pino, G. G., Haddad, A., Scarpa, F., & Dufresne, A. (2019). Extraction and characterization of vascular bundle and fiber strand from date palm rachis as potential bio-reinforcement in composite. *Carbohydrate Polymers*, 222, [114997]. <https://doi.org/10.1016/j.carbpol.2019.114997>

Peer reviewed version

License (if available):  
CC BY-NC-ND

Link to published version (if available):  
[10.1016/j.carbpol.2019.114997](https://doi.org/10.1016/j.carbpol.2019.114997)

[Link to publication record in Explore Bristol Research](#)  
PDF-document

This is the accepted author manuscript (AAM). The final published version (version of record) is available online via Elsevier at <https://doi.org/10.1016/j.carbpol.2019.114997> . Please refer to any applicable terms of use of the publisher.

## University of Bristol - Explore Bristol Research

### General rights

This document is made available in accordance with publisher policies. Please cite only the published version using the reference above. Full terms of use are available: <http://www.bristol.ac.uk/red/research-policy/pure/user-guides/ebr-terms/>

**Extraction and characterization of vascular bundle and fiber strand from date palm rachis as potential bio-reinforcement in composite**

Haithem Boumediri,<sup>a</sup> Abderrezak Bezazi,<sup>a</sup> Gilberto Garcia Del Pino,<sup>b</sup> Abdelkrim Haddad,<sup>a</sup>

Fabrizio Scarpa,<sup>c</sup> Alain Dufresne<sup>d\*</sup>

<sup>a</sup> Laboratoire de Mécanique Appliquée des Nouveaux Matériaux (LMANM), Université 8 Mai 1945, Guelma, Algeria

<sup>b</sup> Department of Mechanical Engineering, State University of Amazonas, Manaus-AM/Brazil, Brazil

<sup>c</sup> Department of Aerospace Engineering, University of Bristol, Queens Building, University Walk BS8 1TR Bristol, UK.

<sup>d</sup> Univ. Grenoble Alpes, CNRS, Grenoble INP, LGP2, F-38000, France.

\* Corresponding author: [alain.dufresne@pagora.grenoble-inp.fr](mailto:alain.dufresne@pagora.grenoble-inp.fr)

**Keywords:** Date palm fibers; Vascular bundles; Fiber strands; Physicochemical analysis; Surface roughness; Tensile properties.

## **Abstract**

Date palm rachis fibers are rich in cellulose, relatively inexpensive, and readily available in Algeria. The aim of this study is to investigate the morphology, structure, mechanical and physicochemical characteristics of both vascular bundles and fiber strands extracted from date palm rachis. The difficulties encountered are associated to the extraction of the fibers without damaging them. The study focuses on the morphological and surface roughness analysis using optical and scanning electron microscopies (SEM), and a non-contact 3D profiler. The chemical, physical and thermal properties have been studied using Fourier-transform infrared (FTIR) spectroscopy, energy dispersive X-ray spectroscopy (EDX), X-ray diffraction (XRD), thermogravimetric analysis (TGA), and differential scanning calorimetry (DSC). The mechanical properties were accessed by tensile tests and they were analyzed using two-parameter Weibull distribution.

## INTRODUCTION

The date palm (*Phoenix dactylifera* L.) is a monocotyledonous flowering plant of the family Palmates (Arecaceae), one of the most important cultivated crops in North Africa and the Middle East (NAME) (Chao & Krueger, 2007). According to Graziano da Silva, General Director of the Food and Agriculture Organization (FAO), the date palm is a symbol of life in NAME. Palm trees play an important role in the economy of the region, with the top ten producing countries accounting for approximately 90% of the global date production (Chandrasekaran & Bahkali, 2013; Ghnimi, Umer, Karim, & Kamal-Eldin, 2017).

Algeria, which is the largest country in Africa and in the Arab world, is among the leading countries in the cultivation and production of palms dates. It is the world's fourth-largest date producer with a total of more than 20 million palm trees and was responsible for more than 14% of the global date production in 2017, with an increase of more than 83% from 2012 to 2017, as confirmed by the Algiers Chamber of Commerce and Industry (Boumediri et al., 2017).

However, as reported in 2011 by (Agoudjil, Benchabane, Boudenne, Ibos, & Fois, 2011) this crop generates a large amount of by-products, such as: (a) the leaves: petiole, rachis, leaflets; (b) the trunk; (c) the products obtained from the bunches (fruit bunch branch of palm, date seeds). It can subsequently produce approximately 40 kg of residue per individual date palm tree annually (Mallaki & Fatehi, 2014). This huge residue amount is not exploited because it is often disposed of by burning or is considered as animal feed or waste and it has been rarely used in handicrafts such as basketry, crates, ropes and traditional construction (Al-Oqla & Sapuan, 2014; Bouguedoura, Bennaceur, Babahani, & Benziouche, 2015).

For researchers interested in lignocellulosic fibers, this agricultural residue is a natural wealth, that can be exploited and valued in different ways such as the reinforcement for biocomposite materials for many application and various industries sectors (Al-oqla,

Alothman, Jawaid, Sapuan, & Es-Saheb, 2014; Anwar, Gulfraz, & Irshad, 2014; Jawaid & Abdul Khalil, 2011; Rabetafika, Bchir, Blecker, & Richel, 2014). This is due to their unique collective advantages, which include easy availability, recyclability, environmental friendliness, biodegradability, low cost, low density, good thermal stability, and reasonable strength and stiffness (Jayaramudu, Guduri, & Varada Rajulu, 2010; Manimaran, Saravanakumar, Mithun, & Senthamaraikannan, 2016).

In fact, recent years have been marked by a sharp increase in studies and work on the use of farming-based waste from the date palm. There are studies which have focused on the outer layer of the date palm stem called mesh, this is due to their availability in the form of fiber with an objective of using these fibers as reinforcement for composites materials (Al-Kaabi, Al-Khanbashi, & Hammami, 2005; Al-Khanbashi, Al-Kaabi, & Hammami, 2005; Alawar, Hamed, & Al-Kaabi, 2009; Alsaed, Yousif, & Ku, 2013; Oushabi et al., 2017). Amroune et al. investigated the mechanical properties of the fiber of date palm fruit branches to the use as potential reinforcement of polymer composites (Amroune et al., 2015). Other investigations are dedicated to the use of date palm wood, petioles and leaves by cutting or hammering to small pieces as material for the manufacture of particleboard (Almi, Lakel, Benchabane, & Kriker, 2015; Saadaoui, Rouilly, Fares, & Rigal, 2013). Also, Khiari et al. studies the application date palm rachis as a source of lignocellulosic biomass for the production of pulp and paper (Khiari, Mhenni, Belgacem, & Mauret, 2010). Unfortunately, there is scarce information available about the utilization and properties of the date palm rachis fibers as a potential eco-friendly bio-reinforcement for bio-composites materials.

According to Agoudjil et al. an amount estimated at more than 800,000 tons of residues is produced per year in Algeria. Botanic experts reported that each date palm tree can produce an average of thirteen new rachis and petioles per year (Agoudjil et al., 2011; Nasser et al., 2016) that corresponds to an average mass of 9.75 kg and 4.4 kg, respectively (Darwish,

Mansour, & Elmously, 2018). Based on this information, the cultivation of date palm can then produce around 200,000 tons of fronds and 90,000 tons of petioles, which are available per year in Algeria. There are more than 950 varieties of date palms in Algeria and the analysis of their production by category shows the variety of Ghars palm tree represents up to 10% of the total production in Algeria (Bouguedoura et al., 2015).

This variety of date palm, with very good commercial value and availability, has not been sufficiently explored, this is why it has been chosen to be the aim of this investigation. The analysis of the rachis cross section morphology leads, to identify for the first time, the existence of two main types of date palms rachis fibers namely: vascular bundles (VBs) and fiber strands (FSs) and showing their location in the rachis. The first part of this work is devoted to developing a new method of extracting of VBs and FSs fibers from the Ghars rachis without any damaging or breaking of them. At the best knowledge of the authors, this is the first investigation permitting to provide a comparison and detailed analysis of the two types of Ghars rachis fibers (VBs and FSs), with emphasis on their physicochemical and thermal properties and their tensile statistic mechanical. Furthermore, their morphology and roughness has been identified and compared. To do this, various techniques has been used to characterize the extracted fibers by scanning electron microscopy (SEM), non-contact 3-D profiler, thermogravimetric analysis (TGA), differential scanning calorimetry (DSC), Fourier-transform infrared (FTIR) spectroscopy, energy dispersive X-ray (EDX) spectroscopy, X-ray diffraction (XRD) and tensile machine. At best knowledge of the authors, the ultimate tensile stress of FSs obtained show the greatest values compared to VBs and also to all the fibers date palm existing in the literature.

## **MATERIALS AND METHODS**

## Materials

There are more than 950 varieties of date palm in Algeria such as Deglet Nour, Ghars, Fergus and Mech Degla (Bouguedoura et al., 2015) and they can be classified into 04 categories from the commercial point of view and their availability:

- *Variety of very good commercial value*, such as: Deglet-Nour, Ghars, Degla-Beida, Tafenoquine, Itima, Mech-Degla, etc ...
- *Ordinary variety*, such as: Arechti, Boudheroua, Taouri, Hamraia and Ksebba, etc...
- *A rare variety, less value, very little available*: Oum-rouah, Oum-Soualef, Oum-aidjet, Oum-Chouika, Azenchi, etc ...
- *A rare variety, not available* (limited number to recently discovered), such as introduced foreign varieties: Zohdi, Halami, Ftemi, Alig, etc ...

Apart from being classified by commercial and availability, another classification for date palm on the basis of the external quality of the fruit of the crops in three classes (Biglari, AlKarkhi, & Easa, 2008):

- Palm produce *soft dates*: which are aqueous, of fibrous texture such as: Ghars, Hamraia, Itima, Zegraia, etc ...
- Palm produce *semi-dry dates* or *semi-soft dates*: which dry up such as: Deglet-Nour, Arechti, Sebaa, Boudraa, Amdj-Zenina, Deglet-Messaoud, etc ...
- Palm produce *dry dates* or *hard dates*: which harden on the tree and have a floury texture, such as: Degla-Beida, Laalami, Lahlou, Deglet-Zohra, Arelou, etc.

In this work, we used leaves of a female palm tree Ghars, this variant of date palm tree represents up to 10% of the total production in Algeria, it is known by its earliness in ripening, its productivity and the ability of this tree to withstand large amounts of alkali and much neglect. This variety of date palm has a very good commercial value and great availability but has not been sufficiently explored. The Ghars rachis used was collected in

November 2017 from a local farm in El-Oued located in the south of Algeria, this farm using brackish water for irrigation. The rachis taken from the palm tree (Figure 1a) was obtained by removing the leaflets and it was cut about 20 cm in length using a knife. The fibers were extracted from the rachis by a manual peeling process. After 150 min of boiling in an autoclave at 120 °C the fibers were extracted from the rachis outer and inner peripheries, and it was observed that it consisted of two types of fibers: vascular bundles (VBs) and fiber strands (FSs) VBs and FSs looks like for the anatomy of pineapple leaves (Mohamed, Sapuan, Shahjahan, & Khalina, 2010). Then, the separated fibers were washed thoroughly using water and then sun dried for one week to ensure maximum moisture removal. Finally, the dried VBs and FSs fibers were collected as shown in Figure 1d for further investigations.



**Figure 1.** Photographs of (a) date palm tree, (b) date palm rachis and leaflets, (c) cut rachis, and (d) vascular bundles (VBs) and fiber strands (FSs).

## **Characterization**

***Morphology and surface elemental composition (SEM–EDX analysis).*** The micrographs were obtained with an environmental scanning electron microscope (SEM) (FEI Quanta 250) equipped with a secondary electron large-field detector (LFD). Micrographs were obtained under low vacuum mode (at a pressure of 40 Pa) under an accelerating voltage between 10 to 20 kV, with a spot size of 3-5 nm and a working distance ranging from 9 to 12 mm. Elemental analysis of the fiber surface was performed by energy dispersive X-Ray



spectroscopy analysis (TEAM-EDX Model) to access the amount of existing elements and results were expressed in weight and atomic percent.

***Topographic characterization.*** The surface roughness of VBs and FSs fibers was optically scanned in 3D using a confocal white light sensor with a high-resolution profilometer (CT-100, Cyber Technologies). The samples were scanned with a step size of 5  $\mu\text{m}$  for an illumination time of 0.5 ms. After scanning, the measured roughness characteristics were analyzed with the SCAN-SUITE software.

***Fourier-transform infrared (FTIR) spectrometry.*** FTIR spectra were obtained with FTIR spectrometer (Nicolet iS10 from Thermo Fisher Scientific equipped with a Golden Gate single reflection ATR accessory) in the wavenumber range 4000-500  $\text{cm}^{-1}$  at a temperature of 25°C and 55% relative humidity. All spectra were collected with a 1  $\text{cm}^{-1}$  wavenumber resolution after 32 continuous scans. Spectrum analysis was performed with Smart OMNI-Transmission accessory (Software OMNIC 9.5).

**Thermogravimetric analysis (TGA).** Thermogravimetric analysis (TGA) and derivative thermogravimetry (DTG) of the fiber samples were carried out using a TGA/DSC 3+ (METTLER TOLEDO). Approximately 10 mg of the sample were filled in ceramic alumina crucible capsule and heated from 30°C to 600°C at a constant heating rate of 10 °C/min, under nitrogen atmosphere at a flow rate of 20 mL/min to prevent any oxidative degradation. The DTG data were also obtained from the analysis using STARe-Evaluation Software.

**Differential scanning calorimetry (DSC).** Differential scanning calorimetry (DSC) analysis was performed using DSC 3+ (METTLER TOLEDO). The equipment was calibrated with aluminum oxide before analysis. The sample (weighing approx. 6 mg) was encapsulated in a hermetic aluminum pan before analysis, and an empty pan was used as reference. The sample was then heated from 30°C to 600°C at a heating rate of 10 °C/min. The nitrogen source was adjusted to a flow of 100 mL/min. All thermograms were analyzed using STARe-Evaluation Software.

**X-ray diffraction (XRD) analysis.** Powder X-ray diffraction (XRD) patterns of the samples were obtained using an X-ray PANalytical Empyrean diffractometer equipped with a PIXcel-3D detector and Cu-K $\alpha$  radiation ( $\lambda = 1.540598\text{\AA}$ ). The generator was operated at 45 kV voltage and 40 mA current. Powder samples were mounted on a sample holder and scanned from 10° to 40° (2 $\theta$  angle range) at a scan rate of 5°/min. The length of the specimen used was 10 mm and the measurement temperature was about 23°C.

The crystallinity index (C.I.) and percentage of crystallinity (%Cr) were calculated based on the Segal method (Segal, Creely, Martin, & Conrad, 1959) using the following equations (1) and (2), respectively:

$$\text{C.I.} = (I_{002} - I_{\text{am}}) / I_{002} \times 100 \quad (\text{Eq.1})$$

$$\text{Cr (\%)} = (I_{002} / (I_{002} + I_{\text{am}})) \times 100 \quad (\text{Eq.2})$$

where  $I_{002}$  is the maximum intensity diffraction of the 002-lattice reflection of the crystallographic form of cellulose at  $2\theta=22^\circ$ , and  $I_{am}$  the minimum intensity of the amorphous material at an angle of approximately  $18.5^\circ$  in the valley between the peaks.

The crystallite size (CS) for VBs and FSs was calculated using Scherrer's equation (Maache, Bezazi, Amroune, Scarpa, & Dufresne, 2017):

$$CS = k \lambda / \beta_{002} \cos \theta \quad (\text{Eq.3})$$

where CS is the crystallite size (nm), k is the Scherrer constant (0.9),  $\lambda$  is the wavelength of X-ray beam ( $1.5405 \text{ \AA}$ ),  $\beta$  is the full width half maxima (FWHM) of peak diffraction (in rad) and  $\theta$  is the diffraction angle. XRD data were deconvoluted using MagicPlot-Pro 2.7.2 software by adjusting one amorphous and three crystalline peak sum for each original curve via Gaussian deconvolution.

**Fiber density.** The density ( $\rho_f$ ) for VBs and FSs fibers was calculated by liquid immersion test using pycnometer with distilled water (ASTM D2320-98) and was determined by the following equation (4):

$$\rho_f = [(m_2 - m_1) / (m_3 - m_1) - (m_4 - m_2)] \rho_{wt} \quad (\text{Eq.4})$$

where  $m_1$ ,  $m_2$ ,  $m_3$ ,  $m_4$  and  $\rho_{wt}$  are the mass of empty pycnometer (g), the mass of pycnometer with fibers (g), the mass of pycnometer with distilled water (g), the mass of pycnometer with fibers and distilled water (g), and the density of distilled water ( $0.997 \text{ g/cm}^3$ ), respectively.

**Technical fiber tensile tests.** The tensile tests were conducted using Zwick/Roell universal testing machine Z2.5 equipped with a 200 N load cell attached to an automatic data acquisition system. 20 samples were analyzed for each group according to ASTM D3822-07 for a fiber length of 30 mm at a constant speed of 1 mm/min. All tests were carried out at a temperature of 23 °C and a relative humidity of approximately 45%. The cross-sectional area was evaluated from the diameter measured using an optical microscope (Motic-BA310 Met, Motic Images Plus 2.0 software) at three different points along the effective fiber length. The statistical analysis of tensile strength values has been analyzed by two parameters Weibull distribution model. The obtained results were treated by Minitab software.

## **RESULTS AND DISCUSSION**

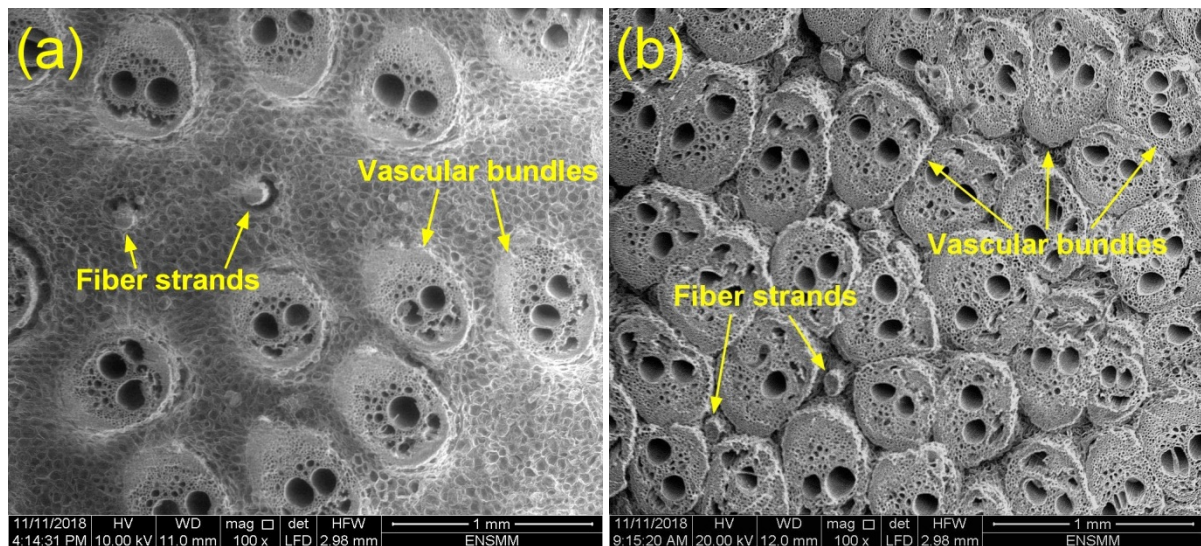
### **Morphological analysis**

Figures 2a and 2b show SEM micrographs of the cross-section at the base and 20 cm before the tip of the date palm rachis, respectively. The micrographs clearly show a gathering of several fibers dispersed and separated by chlorenchyma cells. However, there is a clear difference in the microstructure of these fibers, which can be classified into two types, the first called vascular bundle (VBs) which is the thicker one and that appears in the middle of the main voids, while the second called fiber strand (FSs) is the thinnest that do not contain any main voids. It is worth noting that the parenchyma cells of the base rachis are much denser compared to the tip from the rachis of date palm.

Figures 2c and 2d display the cross-section of VBs and FSs from the rachis of date palm, respectively. The microstructural observation carried out for VBs showed that the surface area is elliptical nearly circular in shape, the VBs being composed of two main voids with diameter ranging from 100 to 150  $\mu\text{m}$  with a large number of spherical microfibrils with a smaller diameter in the range 6-22  $\mu\text{m}$ , aligned and bonded together by lignin, pectin and other non-cellulosic materials (Manimaran, Senthamaraikannan, Sanjay, Marichelvam, &

Jawaid, 2018). FSs are composed of several individual microfibrils with a diameter in the range 4 to 12  $\mu\text{m}$ , compactly arranged to form a technical fiber whose shape is approximately cylindrical and whose diameter was found in the range 80 to 120 microns.

The SEM micrographs of the surface (longitudinal direction) for VBs and FSs are depicted in Figures 2e and 2f, respectively. The presence of some impurities randomly distributed is observed on the surface of VBs and FSs fibers, their existence resulting from the extraction technique. The fiber structure exhibits an alignment in the direction of the fiber axis, in the shape of a regularly distributed semi-rectangular and square tray, along with the length of the lines on the surface of the fibers. Further, it shows small void holes or pits not uniformly spaced and it has the shape of an almost circular elliptical at the surface. In general, this type of structure is similar to other vascular fiber bundles such as arundo fibers (Fiore, Scalici, & Valenza, 2014) and to fiber strands like banana fibers (Kambli, Basak, Samanta, & Deshmukh, 2016).



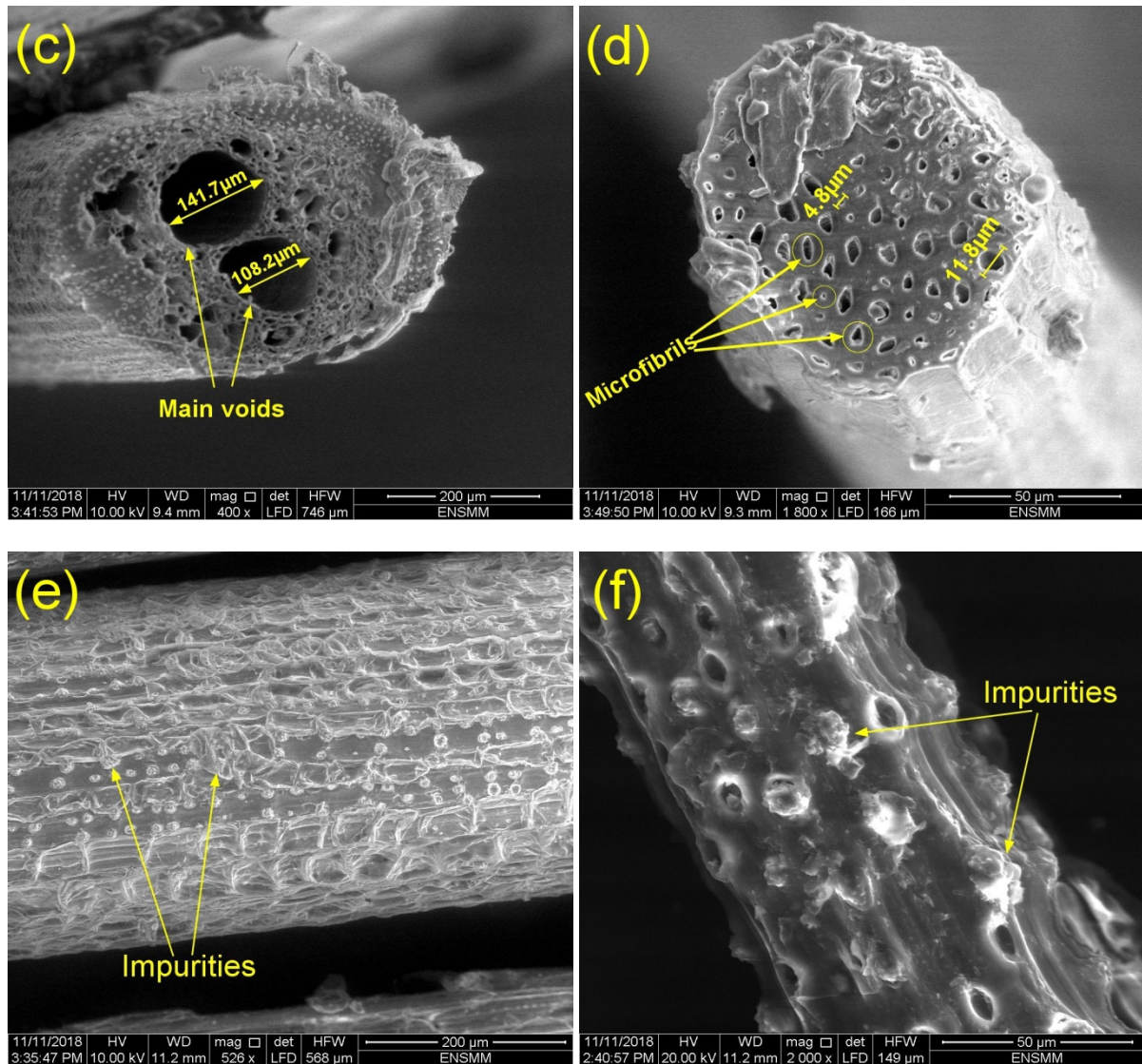


**Figure 2.** SEM micrographs of the cross-section at: (a) the base of the rachis, and (b) 20 cm before the tip of the rachis. SEM micrographs of the cross-section for (c) VBs (d) FSs and longitudinal view for (e) VBs, and (f) FSs.

### EDX analysis

Figures 3a and 3b show the spectral imaging generated by energy dispersive X-ray spectroscopy (EDX) for VBs and FSs, respectively. The fibers consist of elements such as carbon (C), oxygen (O), small amounts of sodium (Na), aluminum (Al), silicon (Si) and traces of chlorine (Cl), potassium (K), calcium (Ca) and the existence of sulfur (S) only in FSs fibers.

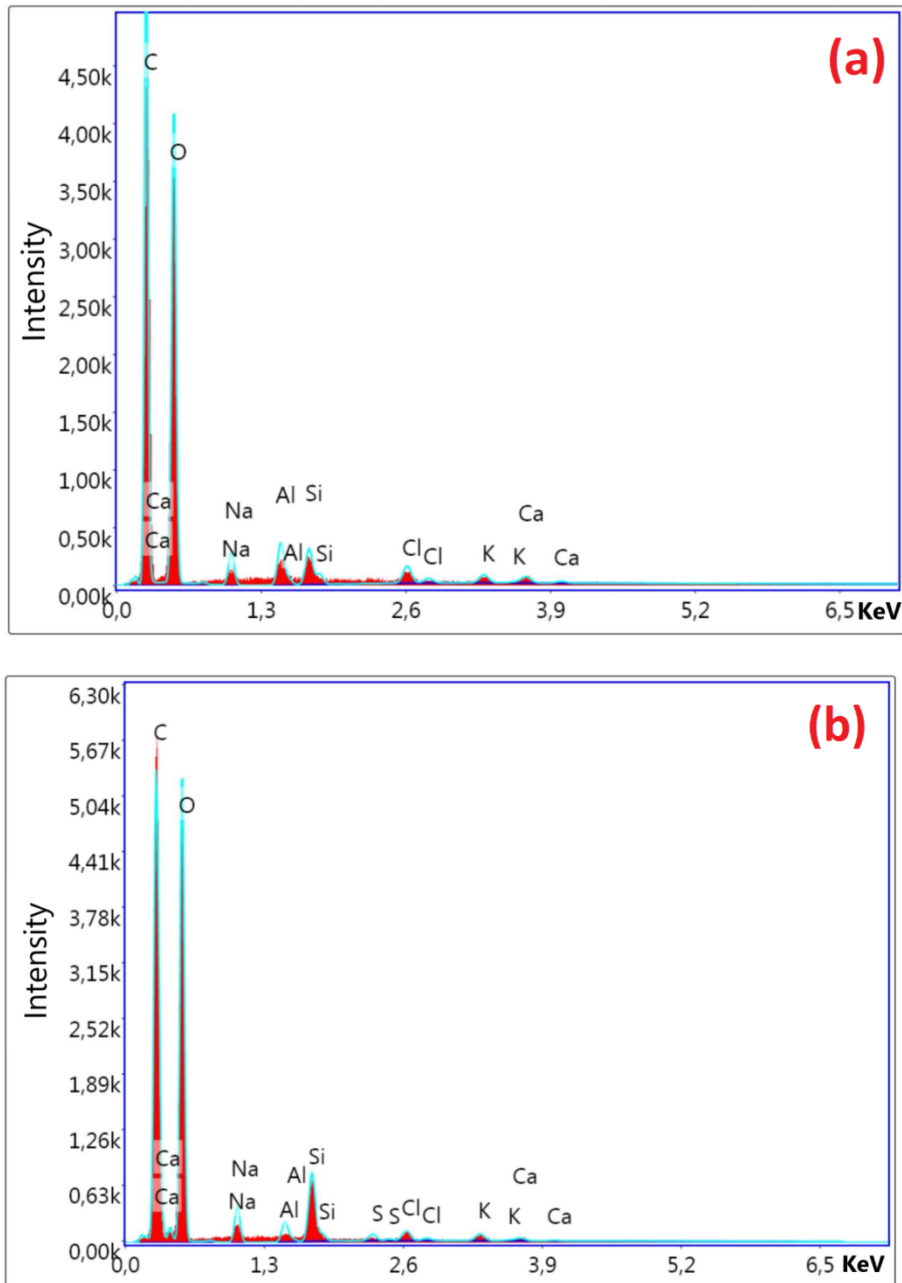


**Figure 3.** EDX analysis for (a) VBs and (b) FSs.

Table 1 reports the results for the weight content and atomic content calculated from the peak areas for all elements. It indicates a similar composition for both fibers. Carbon and oxygen are the main constituents because they are the main components for natural fiber structures (Kambli et al., 2016), that corresponds to the known chemical composition of lignocellulosic fibers.

**Table 1.** Weight (W%) and atomic percentage (A%) for VBs and FSs fibers compared to other

lignocellulosic fibers.

Fiber		Element										Reference
		C	O	Na	Al	Si	Cl	S	Mg	K	Ca	
Vascular bundles	W%	50.14	46.41	1.85	0.86	0.47	0.14			0.06	0.05	Present work
	A%	57.88	40.22	1.12	0.44	0.23	0.06			0.02	0.02	
Fiber strands	W%	50.1	46.21	2.03	0.41	0.97	0.11	0.07		0.07	0.04	
	A%	57.89	40.09	1.22	0.21	0.48	0.04	0.03		0.03	0.01	
Furcraea foetida	W%	66.34	72.50									(Manimaran et al., 2018)
	A%	33.57	27.50									
Cornhusk fiber	W%	62.54	36.80			0.20			0.13		0.33	(Kambli et al., 2016)
	A%	69.17	30.56			0.10			0.07		0.11	
Cotton fiber	W%	46.1	53.2									
	A%	53.9	46.8									
Jute fiber	W%	55.68	43.89			0.11		0.18				
	A%	62.72	37.11			0.06		0.08				

### Surface roughness analysis

Figures 4a and 4b show the 3D roughness surface texture, 2D line diagram for roughness measurement and profilometry results conducted according to ISO 4287 for VBs and FSs fibers, respectively. The visual inspection of 3D topographic images makes it easy to observe the variation in peak value on the surface represented by red color because of the impurities, inorganic substances and the existence of lignin (Manimaran et al., 2018). The area of valleys found in the 3D roughness surface texture (blue color) is due to the presence of voids in VBs and holes or pits in FSs.



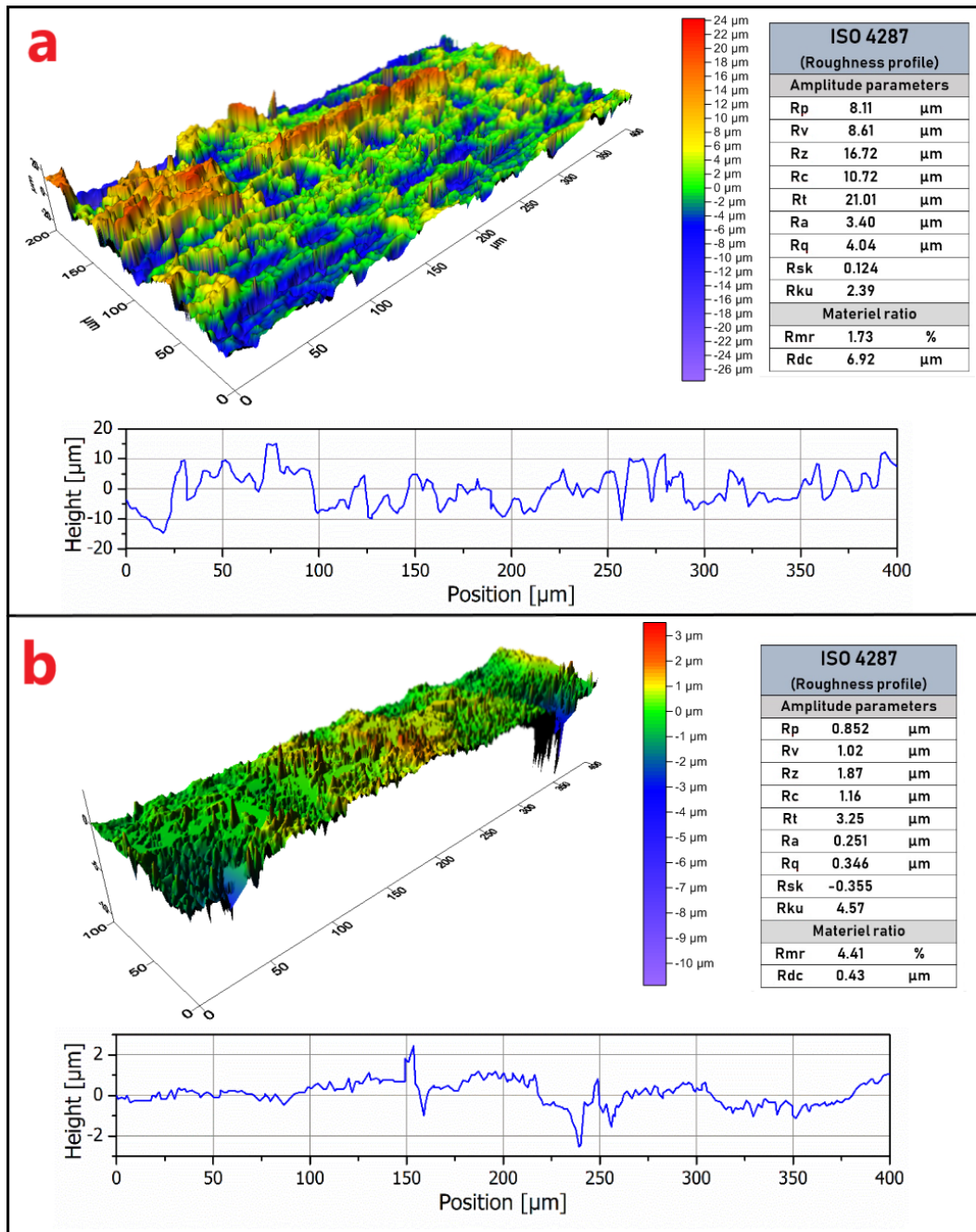


**Figure 4.** 3D surface roughness and 2D line diagram for roughness for (a) VBs and (b) FSs. The 2D line diagram for VBs and FSs show a non-uniform surface roughness along the fiber length. The profilometry results were evaluated and found to be as follow: for VBs ( $R_a = 3.40 \mu\text{m}$ ,  $R_z = 16.72 \mu\text{m}$ ,  $R_q = 4.04 \mu\text{m}$ ,  $R_t = 21.01 \mu\text{m}$ ) and it was lowest for FSs ( $R_a = 0.251 \mu\text{m}$ ,  $R_z = 1.87 \mu\text{m}$ ,  $R_q = 0.346 \mu\text{m}$ ,  $R_t = 3.25 \mu\text{m}$ ). The surface roughness for VBs was higher than for other natural fibers like  $R_a = 0.613 \mu\text{m}$  for *Coccinia grandis* stem fiber (Jebadurai, Raj, Sreenivasan, & Binoj, 2018),  $R_a = 0.611 \mu\text{m}$  for Veldt-grape stem fiber

(Mayandi et al., 2015) and  $R_a = 0.625 \mu\text{m}$  for *Cyperus pangorei* fibers (Mayandi, Rajini, Pitchipoo, Jappes, & Rajulu, 2016), but for FSs it was slightly lower. It was reported that the surface roughness is one of the important properties for enhancing mechanical interlocking between fiber and matrix when used as reinforcement in composite materials (Maache et al., 2017).

### **FTIR analysis**

The FTIR spectra recorded for VBs and FSs of date palm rachis are represented in Figure 5a. Both fibers presented the typical vibration bands of different chemical functional groups of lignin, hemicellulose and cellulose. The strong and broad peak at  $3346 \text{ cm}^{-1}$  is associated with the O-H stretching vibration and hydrogen bond of the hydroxyl groups (Amroune et al., 2015). The double peak observed at  $2925$  and  $2854 \text{ cm}^{-1}$  are assigned to  $\text{CH}_2$  asymmetrical and symmetrical stretching, respectively. The absorption band centered at  $1734 \text{ cm}^{-1}$  can be attributed to the C=O group and stretching vibration of ester group in hemicellulose (Bezazi, Belaadi, Bouchak, Scarpa, & Boba, 2014). The small band at  $1646 \text{ cm}^{-1}$  corresponds to the O-H bending of absorbed water. Following three peaks are characteristic of lignin:  $1604 \text{ cm}^{-1}$  (aromatic skeletal vibration of lignin plus C=O stretching),  $1508 \text{ cm}^{-1}$  (C=C stretching of aromatic skeletal vibration of Lignin),  $1456 \text{ cm}^{-1}$  (C-H deformation (asymmetric) and aromatic vibration in lignin) (Amroune et al., 2015; Saravanakumar, Kumaravel, Nagarajan, & Moorthy, 2014). The absorbance at  $1423 \text{ cm}^{-1}$  is attributed to the presence of C-H deformation in lignin and  $\text{CH}_2$  symmetric bending in cellulose (Maache et al., 2017). The absorption band at  $1373 \text{ cm}^{-1}$  is assigned to the bending vibration of the C-H group of the aromatic ring in hemicellulose and cellulose (Bezazi et al., 2014). The absorbance at  $1319 \text{ cm}^{-1}$  is attributed to the  $\text{CH}_2$  rocking vibration in cellulose (Saravanakumar et al., 2014). The tiny peak at  $1241 \text{ cm}^{-1}$  is assigned to the C-O stretching of acetyl group in lignin (Bezazi et al., 2014). The two peaks observed at  $1160 \text{ cm}^{-1}$  and  $1033 \text{ cm}^{-1}$  are attributed to the C-O-C

asymmetric stretching vibration and C–O stretching ring in cellulose and hemicellulose, respectively (Saravanakumar et al., 2014). A small peak at  $897\text{ cm}^{-1}$  is attributed to the  $\beta$ -glycosidic linkages between the monosaccharides. The small absorption peak at  $605\text{ cm}^{-1}$  is associated with C-OH out of plane bending in cellulose (Fiore et al., 2014).

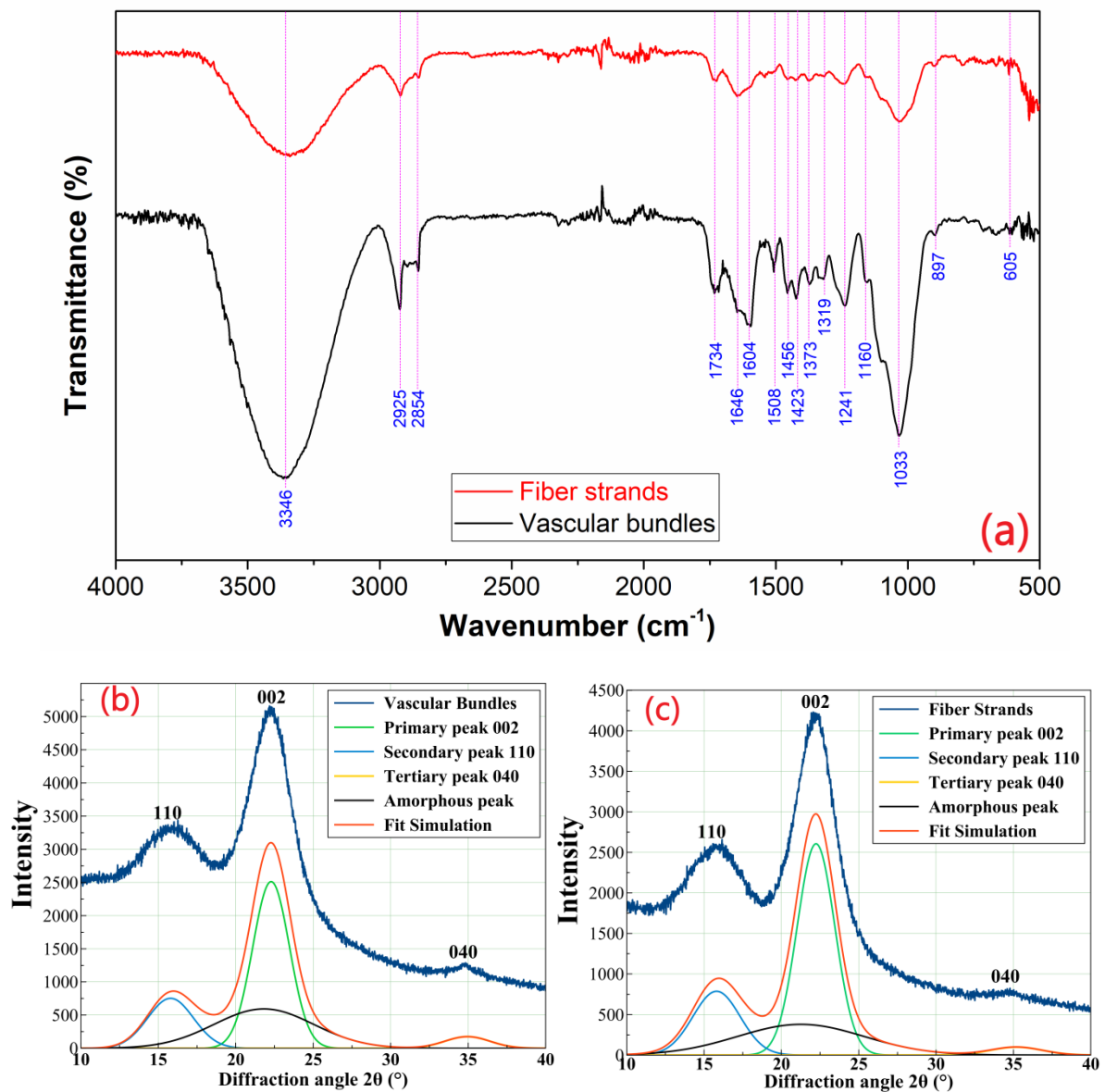


**Figure 5.** (a) FTIR spectra for VBs and FSs, and XRD patterns for (b) VBs and (c) FSs.

### XRD analysis

The diffraction patterns obtained for VBs and FSs between  $10$  and  $40^\circ$  are shown in Figures 5b and 5c, respectively. The deconvolution of the X-ray diffraction profiles showed the

presence of three peaks and an amorphous bump. For both VBs and FSs the highest intensity peak was observed at  $2\theta = 22.2^\circ$ , average intensity peak at  $2\theta = 15.86^\circ$  and a peak of low intensity at  $2\theta = 35^\circ$ , which were assigned to the (002), (10 $\bar{1}$ ), and (040) crystallographic planes (Jebadurai et al., 2018).

The crystallinity index (C.I.) was found to be 47.82% and 56.68% for VBs and FSs samples, respectively, which means that FSs exhibit a better order of cellulose crystals at the fiber axis compared to VBs. On the other hand, the percentage of crystallinity (%Cr) for VBs and FSs was found equal to 65.71% and 69.77%, respectively. In addition, the crystallite size (CS) for VBs and FSs was calculated using Scherrer's equation and the value was found to be 5.78 nm and 5.63 nm, respectively, which is smaller than the value reported for *Furcraea foetida* (28.36 nm), *Prosopis juliflora* bark (15 nm), but higher than for *Juncus effusus L.* (3.6 nm) and *Coccinia grandis* stem (1.91 nm) as reported by (Jebadurai et al., 2018; Maache et al., 2017; Manimaran et al., 2018; Saravanakumar, Kumaravel, Nagarajan, Sudhakar, & Baskaran, 2013). The obtained results are summarized in Table 2 and compared to (Roy et al., 2012; Wei & Meyer, 2015)

**Table 2.** Calculated and experimental crystalline parameters from XRD diffractograms of fibers.

Type of fiber	Peak position ( $^\circ$ )	FWHM (rad)	Area (%)	Crystallinity (%)	Crystalline index (%)	Crystallite size (nm)	Reference
Vascular bundles	15.79	1.74	2789.23	65.71	47.82	5.78	Present work
	22.28	1.40	7487.62				
Fiber strands	15.81	1.79	3006.61	69.77	56.68	5.63	
	22.24	1.44	7980.62				
Sisal fiber	16,81	4.89		77.6	71.2	3.37	(Wei & Meyer, 2015)
	22,31	3.37					
Jute fiber	15.62	4,23	42.05	53.7		2.78	(Roy et al., 2012)
	23.36	2.89	57.94				

## **TGA analysis**

Thermogravimetric analysis (TGA) and derivative thermogravimetry (DTG) are thermal analysis techniques used to measure the weight loss of a material when heated, i.e. to assess its thermal stability, and characterize its decomposition temperature.

Figure 6 presents the TG and DTG curves for VBs and FSs, which show four weight loss stages. The first stage associated with a small weight loss (8.10%) for VBs and (7.00%) for FSs, corresponds to the dehydration phase that was observed in the temperature range 30-120 °C. This stage was attributed to the evaporation of adsorbed moisture, which is related to the hydrophilic nature of lignocellulosic materials (Fiore et al., 2014). Then, it can be concluded that both VBs and FSs can be considered thermally stable up to 230 °C and 220, respectively. The thermal stability of lignocellulosic fibers is important for the processing and usage of these materials as a reinforcement in biocomposites (Maache et al., 2015). In the second stage, the degradation of hemicelluloses was recorded in the temperature range 220-325 °C with a weight loss of 29% for VBs and in the temperature range 220-300 °C with a weight loss of 22% for FSs (Martin, Martins, Da Silva, & Mattoso, 2010; Saravanakumar et al., 2013). It is confirmed by the observation of a peak in the DTG curves at 296 °C for VBs and 280 °C for FSs. Afterward, the major weight loss occurred rapidly in the third degradation stage, corresponding to the decomposition of cellulose in the temperature range 325-490 °C associated with a weight loss of 39.00% for VBs and in the temperature range 300-480 °C with a higher weight loss of 41.51% for FSs. The DTG plots showed distinct peaks at 360 °C for VBs and 345 °C for FSs (Jebadurai et al., 2018). Lastly, the final stage corresponding to the decomposition of lignin was observed in the temperature range 400-485 °C with a small weight loss for VBs (10%) and in the temperature range 380-465 °C with a smaller weight loss for FSs (7%) (Roy et al., 2012). In addition, amounts of charred residues were observed for VBs (16.66%) and FSs (18.28%).

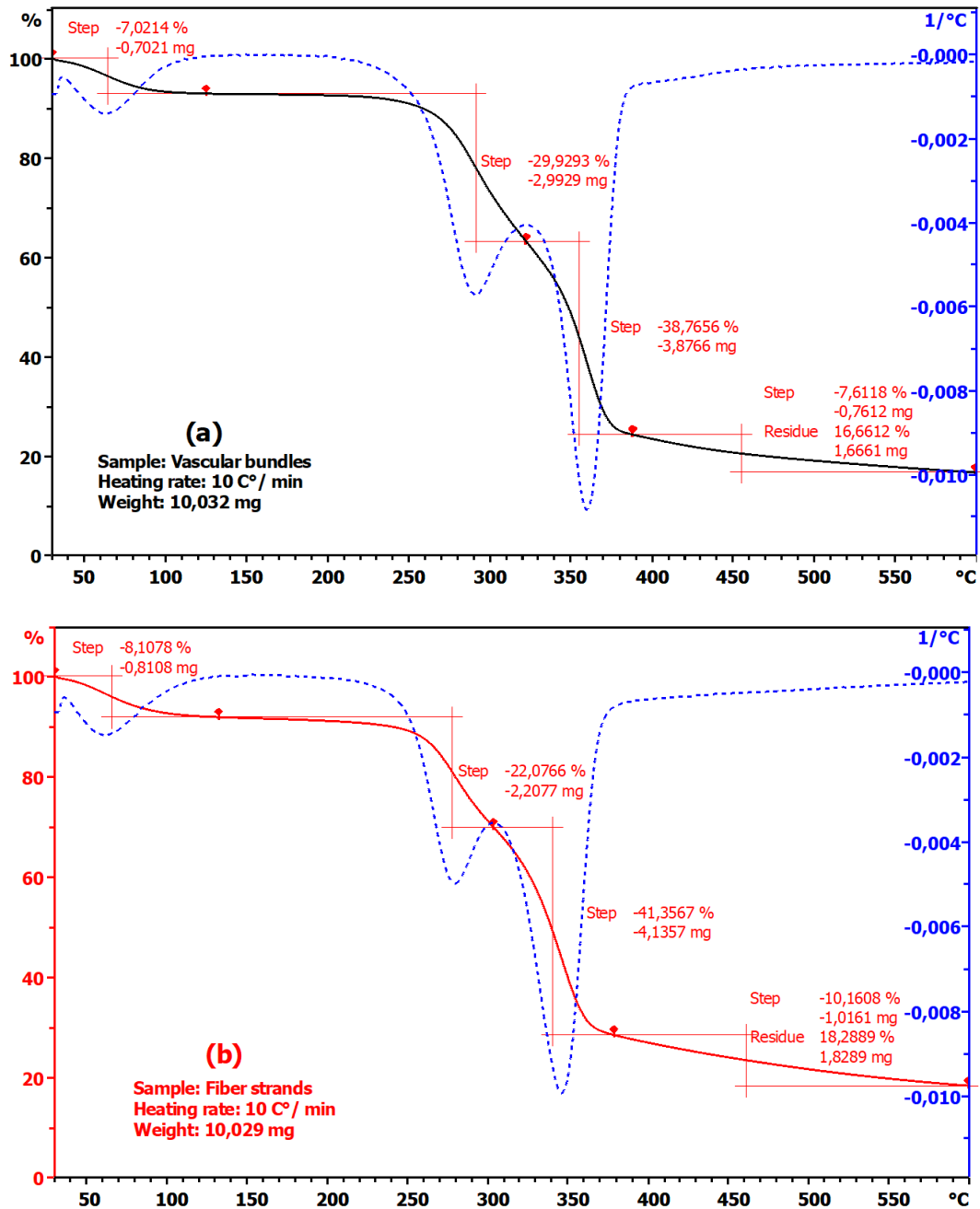
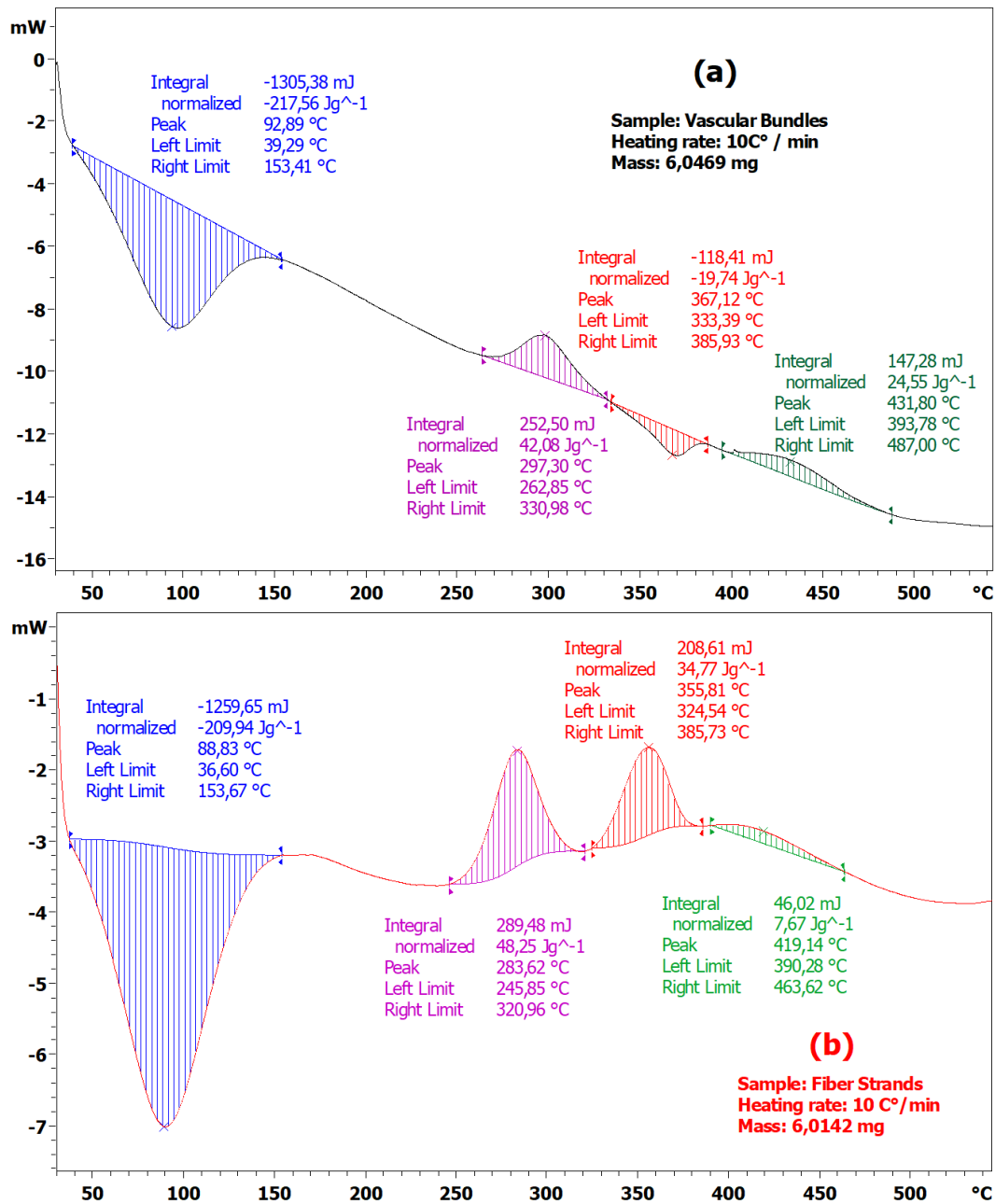


Figure 6. TGA/DTG curves for (a) VBs and (b) FSs.

### DSC analysis

Differential scanning calorimetry (DSC) analysis was carried out for both VBs and FSs for determining its thermal behavior. DSC analysis allows observing physical changes through the absorption and release of thermal energy during heating, which allows the identification of thermal transitions. Figure 7 shows the DSC curves obtained for VBs and FSs presenting the endothermic and exothermic processes where some differences can be noted. The first

endothermic peak was centered at 92°C and 88°C for VBs and FSs, respectively. It corresponds to the loss/evaporation of absorbed water (Belaadi, Bezazi, Bouchak, Scarpa, & Zhu, 2014). The corresponding enthalpy calculated by integrating the peak was 217 J/g and 209 J/g for VBs and FSs, respectively.



**Figure 7.** DSC curves for (a) VBs and (b) FSs.

The exothermic peak observed at 297°C and 283°C for VBs and FSs, respectively, is mainly due to the degradation of hemicelluloses present in the samples which is associated with an

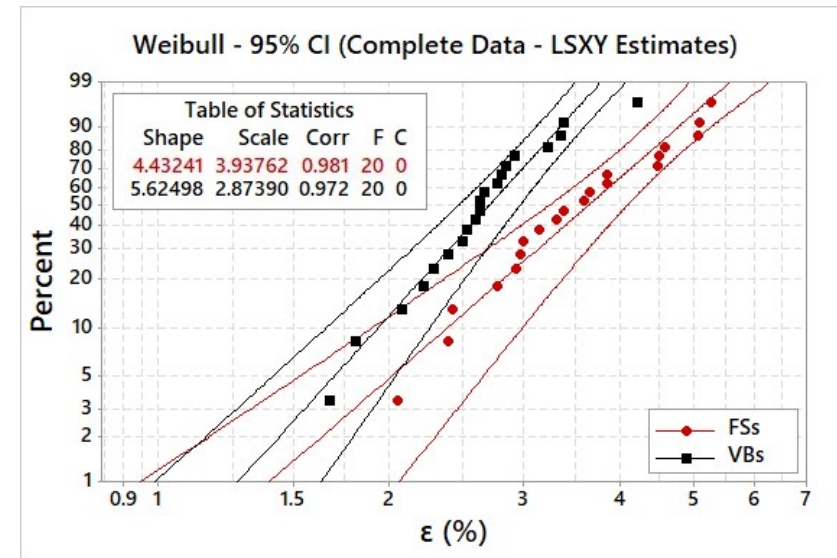
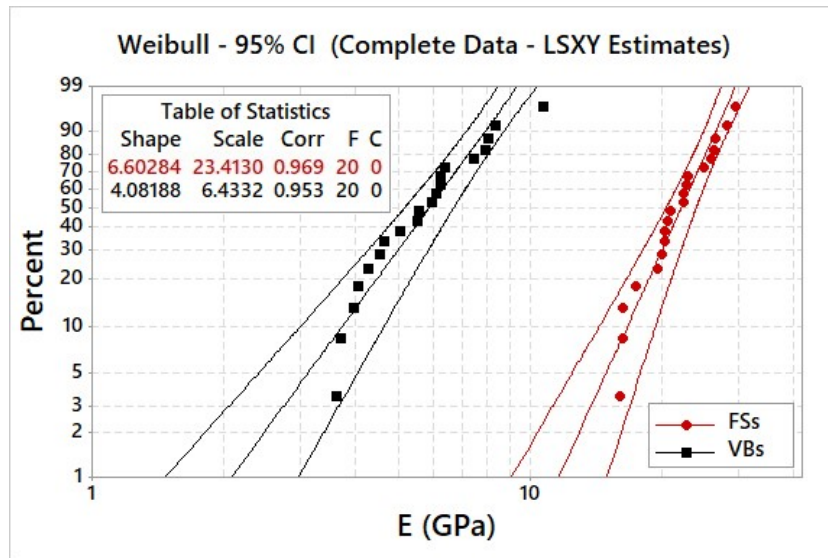
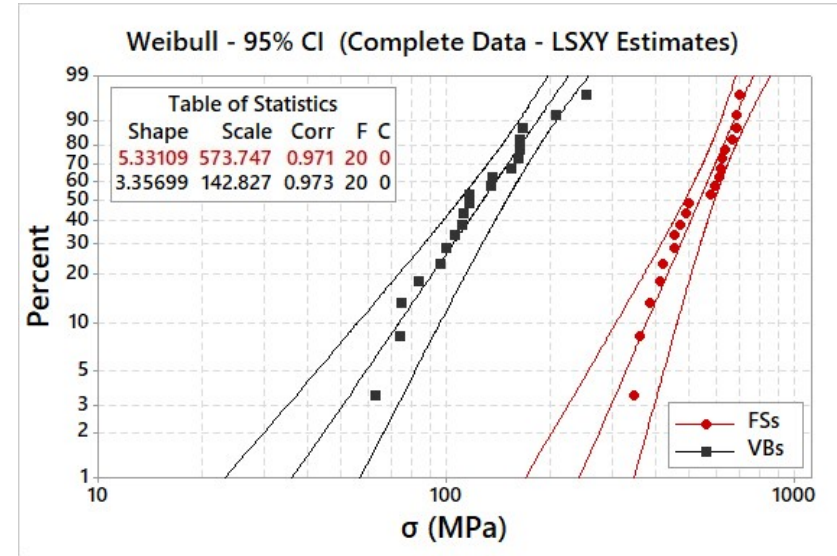
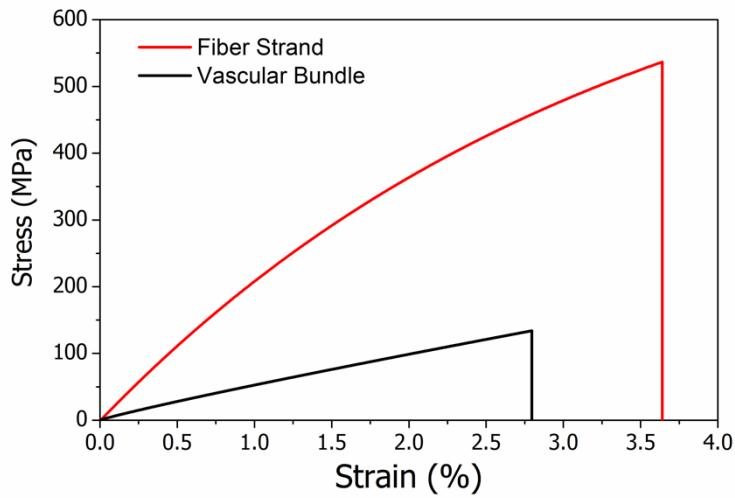
enthalpy of 42 J/g for VBs and 48 J/g for FSs (Martin et al., 2010). Then a different behavior is observed between VBs and FSs with an endothermic peak around 367°C for the former and exothermic peak around 355°C for the later. According to DTG results this signal should correspond to the degradation of cellulose and the associated enthalpy is 19 J/g for VBs while it is 34 J/g for FSs (Roy et al., 2012). Finally, a small exothermic peak observed at 431 °C for VBs and 419 °C for FSs is mainly due to the thermal decomposition of lignin, were a much higher enthalpy (24 J/g) is reported for VBs than for FSs (7 J/g).

### **Technical fiber tensile tests and statistical analysis**

The typical stress-strain curves for VBs and FSs under tensile tests behave quasi-linearly and non-linearly, respectively, until failure (Figure 8a). It is worth noting that the mechanical properties of FSs are largely better compared to VBs. Due to the dispersion in the obtained results, it was deemed necessary to analyze them statistically using two-parameters Weibull distribution fit plots of the test data for all the 20 trials with 95% confidence level curves for tensile strength, Young's modulus and strain at failure. The results are presented in Figure 8b, 8c, and 8d, respectively, for VBs and FSs having an average diameter of  $520\pm 72\mu\text{m}$  and  $88\pm 12\mu\text{m}$ , respectively, with low density of  $0.914\text{ g/cm}^3$  and  $0.922\text{ g/cm}^3$ , respectively. The Weibull distribution provides a reasonable approximation of the experimental data for evaluating the mechanical properties of different natural fibers. The experimental results obtained for VBs and FSs were found to be  $129.1\pm 47.3\text{ MPa}$  and  $530.5\pm 115.2\text{ MPa}$  for the ultimate tensile strength,  $5.88\pm 1.84\text{ GPa}$  and  $21.90\pm 3.96\text{ GPa}$  for the Young's modulus, and  $2.67\pm 0.57\%$  and  $3.60\pm 0.95$  for the strain at failure, respectively. These values are very close to the ones obtained by Weibull distribution: ultimate tensile strength  $142.8\text{ MPa}$  and  $573.7\text{ MPa}$ , Young's modulus  $6.43\text{ GPa}$  and  $23.41\text{ GPa}$ , and strain at failure  $2.87\%$  and  $3.93\%$ , respectively, with precision adjustment R-Squared values ranging from 0.953 to 0.981.



In addition, the tensile strength value obtained for VBs was similar to the one reported for agave fiber ( $135\pm 71$  MPa) (Bezazi et al., 2014), fiber fruit bunch branch of palm date ( $117\pm 35$  MPa) (Amroune et al., 2015) and *Juncus effusus L.* ( $113\pm 36$  MPa) (Maache et al., 2017). It is much higher for FSs ( $530.5\pm 115.2$  MPa), which value is close to the one reported for pineapple leaf fiber strands (506 MPa) (Mohamed et al., 2010), *Prosopis juliflora* bark fiber ( $558\pm 13.4$  MPa) (Saravanakumar et al., 2013) and sisal fiber (605.86 MPa) (Wei & Meyer, 2015). These results expressly demonstrated that the tensile properties were influenced mainly by the morphological structure and that the presence of the main voids decreases their properties. It can also be seen from the results that the tensile properties are increased with the augmentation of the crystallinity index of fibers.



1

2

3 **Figure 8.** (a) Typical stress–strain curve for VBs and FSs, and two-parameter Weibull distribution for VBs and FSs for (b) tensile strength, (c)  
 4 Young’s modulus, and (d) strain at break.

## 5 CONCLUSION

6 The investigation of the Ghars date palm rachis fibers leads to the main following  
7 conclusions:

8 -The existence of two main types of Ghars date palms rachis fibers have been identify, for the  
9 first time, on the basis of cross-sectional geometry namely: vascular bundles (VBs) and fiber  
10 strands (FSs) and showing their location in the rachis. Also, a new extraction method for  
11 Ghars rachis have been developed without any damaging or breaking it.

12 - The noncontact 3D profiler observations show that VBs and FSs have a rough surface  
13 ( $R_a=3.40$  and  $R_a= 0.251$ , respectively), which is essential for adhesion to the polymer matrix.

14 - XRD analysis showed that FSs has a higher crystallinity index (56.68%) compared to VBs  
15 (47.82%). In addition, the crystallite size (CS) for VBs and FSs was found to be 5.78 nm and  
16 5.63 nm, respectively.

17 - The main chemical and molecular structure groups were identified by FTIR analysis  
18 showing similar functional groups compared to other lignocellulosic fibers reported in the  
19 literature and EDX indicates similar composition content for both fibers.

20 - TGA and DSC analysis for VBs and FSs show that it can be stable up to 230 °C and 220,  
21 respectively, i.e. it has good thermal stability. The thermal events associated to hemicellulose,  
22 cellulose, and lignin has been determined.

23 - The density was evaluated for at 0.914 g/cm<sup>3</sup> for VBs, which was slightly lower that for FSs  
24 (0.922 g/cm<sup>3</sup>).

25 - The statistical analysis with Weibull distribution function showed a good approximation fit  
26 value with the experimental data obtained. This results clearly indicate that the influence of  
27 the crystallinity index and the effect of the structural morphology of the fibers on the tensile  
28 properties. In other words, the high crystallinity index leads to have better tensile properties.

29 - The tensile strength for FSs was found to be 530.5 ±115.2 MPa, i.e. more than 4 times than

30 for VBs ( $129.1 \pm 47.3$  MPa), and the Young's modulus of FSs and VBs was  $21.90 \pm 3.96$  GPa,  
31  $5.88 \pm 1.84$  GPa, respectively.  
32 - The mechanical properties obtained show great properties of ultimate tensile stress FSs  
33 compared to VBs and also to all the fibers date palm existing in the literature. Therefore, the  
34 fibers investigated show great potential for use as reinforcement for biocomposites in diverse  
35 engineering applications.

36

## 37 REFERENCES

- 38 Agoudjil, B., Benchabane, A., Boudenne, A., Ibos, L., & Fois, M. (2011). Renewable  
39 materials to reduce building heat loss: Characterization of date palm wood. *Energy and*  
40 *Buildings*, 43(2–3), 491–497. <https://doi.org/10.1016/j.enbuild.2010.10.014>
- 41 Al-Kaabi, K., Al-Khanbashi, A., & Hammami, A. (2005). Date Palm Fibers as Polymeric  
42 Matrix Reinforcement : DPF / Polyester Composite Properties. *POLYMER*  
43 *COMPOSITES*, 26, 604–613. <https://doi.org/10.1002/pc.20130>
- 44 Al-Khanbashi, A., Al-Kaabi, K., & Hammami, A. (2005). Date palm fibers as polymeric  
45 matrix reinforcement: Fiber characterization. *Polymer Composites*, 26(4), 486–497.  
46 <https://doi.org/10.1002/pc.20118>
- 47 Al-oqla, F. M., Alothman, O. Y., Jawaid, M., Sapuan, S. M., & Es-Saheb, M. H. (2014).  
48 Processing and Properties of Date Palm Fibers and Its Composites. In *Biomass and*  
49 *Bioenergy* (pp. 1–25). Springer, Cham. <https://doi.org/10.1007/978-3-319-07641-6>
- 50 Al-Oqla, F. M., & Sapuan, S. M. (2014). Natural fiber reinforced polymer composites in  
51 industrial applications: Feasibility of date palm fibers for sustainable automotive  
52 industry. *Journal of Cleaner Production*, 66, 347–354.  
53 <https://doi.org/10.1016/j.jclepro.2013.10.050>
- 54 Alawar, A., Hamed, A. M., & Al-Kaabi, K. (2009). Characterization of treated date palm tree  
55 fiber as composite reinforcement. *Composites Part B: Engineering*, 40(7), 601–606.  
56 <https://doi.org/10.1016/j.compositesb.2009.04.018>
- 57 Almi, K., Lakel, S., Benchabane, a., & Kriker, a. (2015). Characterization of Date Palm  
58 Wood Used as Composites Reinforcement. *Acta Physica Polonica A*, 127(4), 1072–  
59 1074. <https://doi.org/10.12693/APhysPolA.127.1072>
- 60 Alsaeed, T., Yousif, B. F., & Ku, H. (2013). The potential of using date palm fibres as

61 reinforcement for polymeric composites. *Materials and Design*, 43, 177–184.  
62 <https://doi.org/10.1016/j.matdes.2012.06.061>

63 Amroune, S., Bezazi, A., Belaadi, A., Zhu, C., Scarpa, F., Rahatekar, S., & Imad, A. (2015).  
64 Tensile mechanical properties and surface chemical sensitivity of technical fibres from  
65 date palm fruit branches (*Phoenix dactylifera* L.). *Composites Part A: Applied Science*  
66 *and Manufacturing*, 71(November), 98–106.  
67 <https://doi.org/10.1016/j.compositesa.2014.12.011>

68 Anwar, Z., Gulfraz, M., & Irshad, M. (2014). Agro-industrial lignocellulosic biomass a key to  
69 unlock the future bio-energy: A brief review. *Journal of Radiation Research and*  
70 *Applied Sciences*, 7(2), 163–173. <https://doi.org/10.1016/j.jrras.2014.02.003>

71 Belaadi, A., Bezazi, A., Bourchak, M., Scarpa, F., & Zhu, C. (2014). Thermochemical and  
72 statistical mechanical properties of natural sisal fibres. *Composites Part B: Engineering*,  
73 67, 481–489. <https://doi.org/10.1016/j.compositesb.2014.07.029>

74 Bezazi, A., Belaadi, A., Bourchak, M., Scarpa, F., & Boba, K. (2014). Novel extraction  
75 techniques, chemical and mechanical characterisation of *Agave americana* L. natural  
76 fibres. *Composites Part B: Engineering*, 66, 194–203.  
77 <https://doi.org/10.1016/j.compositesb.2014.05.014>

78 Biglari, F., AlKarkhi, A. F. M., & Easa, A. M. (2008). Antioxidant activity and phenolic  
79 content of various date palm (*Phoenix dactylifera*) fruits from Iran. *Food Chemistry*,  
80 107(4), 1636–1641. <https://doi.org/10.1016/J.FOODCHEM.2007.10.033>

81 Bouguedoura, N., Bennaceur, M., Babahani, S., & Benziouche, S. E. (2015). Date Palm  
82 Status and Perspective in Algeria. In *Date Palm Genetic Resources and Utilization:*  
83 *Volume 1: Africa and the Americas* (pp. 1–546). [https://doi.org/10.1007/978-94-017-](https://doi.org/10.1007/978-94-017-9694-1)  
84 9694-1

85 Boumediri, H., Bezazi, A., Haddad, A., Saaidia, A., Scarpa, F., & Dufresne, A. (2017).  
86 Physico-Chemical Characterization of Date Palm leaves (*Phoenix Dactylifera*-L) of  
87 Algeria. In A. J. M. Ferreira, E. Viola, F. Tornabene, & N. Fantuzzi (Eds.), *Mechcomp3:*  
88 *3rd International Conference of Mechanics of Composite* (p. 24). Esculapio.

89 Chandrasekaran, M., & Bahkali, A. H. (2013). Valorization of date palm (*Phoenix*  
90 *dactylifera*) fruit processing by-products and wastes using bioprocess technology -  
91 Review. *Saudi Journal of Biological Sciences*, 20(2), 105–120.  
92 <https://doi.org/10.1016/j.sjbs.2012.12.004>

93 Chao, C. C. T., & Krueger, R. R. (2007). The date palm (*Phoenix dactylifera* L.): Overview  
94 of biology, uses, and cultivation. *HortScience*, 42(5), 1077–1082.

- 95 Darwish, E. A., Mansour, Y. M., & Elmously, H. (2018). Date Palm Rachis as a Local and  
96 Renewable Structural Material for Rural Communities in Egypt. *The International*  
97 *Journal of Environmental Science & Sustainable Development*, 2(1), 1–11.  
98 <https://doi.org/10.21625/essd.v2i1.173.g75>
- 99 Fiore, V., Scalici, T., & Valenza, A. (2014). Characterization of a new natural fiber from  
100 *Arundo donax* L. as potential reinforcement of polymer composites. *Carbohydrate*  
101 *Polymers*, 106(1), 77–83. <https://doi.org/10.1016/j.carbpol.2014.02.016>
- 102 Ghnimi, S., Umer, S., Karim, A., & Kamal-Eldin, A. (2017). Date fruit (*Phoenix dactylifera*  
103 L.): An underutilized food seeking industrial valorization. *NFS Journal*, 6, 1–10.  
104 <https://doi.org/10.1016/j.nfs.2016.12.001>
- 105 Jawaid, M., & Abdul Khalil, H. P. S. (2011). Cellulosic/synthetic fibre reinforced polymer  
106 hybrid composites: A review. *Carbohydrate Polymers*, 86(1), 1–18.  
107 <https://doi.org/10.1016/j.carbpol.2011.04.043>
- 108 Jayaramudu, J., Guduri, B. R., & Varada Rajulu, A. (2010). Characterization of new natural  
109 cellulosic fabric *Grewia tilifolia*. *Carbohydrate Polymers*, 79(4), 847–851.  
110 <https://doi.org/10.1016/j.carbpol.2009.10.046>
- 111 Jebadurai, S. G., Raj, R. E., Sreenivasan, V. S., & Binoj, J. S. (2018). Comprehensive  
112 characterization of natural cellulosic fiber from *Coccinia grandis* stem. *Carbohydrate*  
113 *Polymers*, 207, 675–683. <https://doi.org/10.1016/j.carbpol.2018.12.027>
- 114 Kambli, N., Basak, S., Samanta, K. K., & Deshmukh, R. R. (2016). Extraction of Natural  
115 Cellulosic Fibers from Cornhusk and Its Physico-Chemical Properties. *Fibers and*  
116 *Polymers*, 17(5), 687–694. <https://doi.org/10.1007/s12221-016-5416-0>
- 117 Khiari, R., Mhenni, M. F., Belgacem, M. N., & Mauret, E. (2010). Chemical composition and  
118 pulping of date palm rachis and *Posidonia oceanica* - A comparison with other wood and  
119 non-wood fibre sources. *Bioresource Technology*, 101(2), 775–780.  
120 <https://doi.org/10.1016/j.biortech.2009.08.079>
- 121 Maache, M., Bezazi, A., Amroune, S., Scarpa, F., & Dufresne, A. (2017). Characterization of  
122 a novel natural cellulosic fiber from *Juncus effusus* L. *Carbohydrate Polymers*, 171,  
123 163–172. <https://doi.org/10.1016/j.carbpol.2017.04.096>
- 124 Mallaki, M., & Fatehi, R. (2014). Design of a biomass power plant for burning date palm  
125 waste to cogenerate electricity and distilled water. *Renewable Energy*, 63, 286–291.  
126 <https://doi.org/10.1016/j.renene.2013.09.036>
- 127 Manimaran, P., Saravanakumar, S. S., Mithun, N. K., & Senthamaraiannan, P. (2016).  
128 Physicochemical properties of new cellulosic fibers from the bark of *Acacia arabica*.

129 *International Journal of Polymer Analysis and Characterization*, 21(6), 548–553.  
130 <https://doi.org/10.1080/1023666X.2016.1177699>

131 Manimaran, P., SenthamaraiKannan, P., Sanjay, M. R., Marichelvam, M. K., & Jawaid, M.  
132 (2018). Study on characterization of *Furcraea foetida* new natural fiber as composite  
133 reinforcement for lightweight applications. *Carbohydrate Polymers*, 181, 650–658.  
134 <https://doi.org/10.1016/j.carbpol.2017.11.099>

135 Martin, A. R., Martins, M. A., Da Silva, O. R. R. F., & Mattoso, L. H. C. (2010). Studies on  
136 the thermal properties of sisal fiber and its constituents. *Thermochimica Acta*, 506(1–2),  
137 14–19. <https://doi.org/10.1016/j.tca.2010.04.008>

138 Mayandi, K., Rajini, N., Pitchipoo, P., Jappes, J. T. W., & Rajulu, A. V. (2016). Analysis and  
139 Extraction and characterization of new natural lignocellulosic fiber *Cyperus pangorei*.  
140 *International Journal of Polymer Analysis and Characterization*, 21(2), 175–183.  
141 <https://doi.org/10.1080/1023666X.2016.1132064>

142 Mayandi, K., Rajini, N., Pitchipoo, P., Sreenivasan, V. S., Jappes, J. W., & Alavudeen, A.  
143 (2015). A comparative study on characterisations of *Cissus quadrangularis* and *Phoenix*  
144 *reclinata* natural fibres. *Journal of Reinforced Plastics and Composites*, 34(4), 269–280.  
145 <https://doi.org/10.1177/0731684415570045>

146 Mohamed, A. R., Sapuan, S. M., Shahjahan, M., & Khalina, A. (2010). Effects of simple  
147 abrasive combing and pretreatments on the properties of pineapple leaf fibers (palf) and  
148 palf-vinyl ester composite adhesion. *Polymer - Plastics Technology and Engineering*,  
149 49(10), 972–978. <https://doi.org/10.1080/03602559.2010.482072>

150 Nasser, R., Salem, M., Hiziroglu, S., Al-Mefarrej, H., Mohareb, A., Alam, M., & Aref, I.  
151 (2016). Chemical Analysis of Different Parts of Date Palm (*Phoenix dactylifera* L.)  
152 Using Ultimate, Proximate and Thermo-Gravimetric Techniques for Energy Production.  
153 *Energies*, 9(5), 374. <https://doi.org/10.3390/en9050374>

154 Oushabi, A., Sair, S., Oudrhiri Hassani, F., Abboud, Y., Tanane, O., & El Bouari, A. (2017).  
155 The effect of alkali treatment on mechanical, morphological and thermal properties of  
156 date palm fibers (DPFs): Study of the interface of DPF–Polyurethane composite. *South*  
157 *African Journal of Chemical Engineering*, 23, 116–123.  
158 <https://doi.org/10.1016/j.sajce.2017.04.005>

159 Rabetafika, H. N., Bchir, B., Blecker, C., & Richel, A. (2014). Fractionation of apple by-  
160 products as source of new ingredients: Current situation and perspectives. *Trends in*  
161 *Food Science and Technology*, 40(1), 99–114. <https://doi.org/10.1016/j.tifs.2014.08.004>

162 Roy, A., Chakraborty, S., Kundu, S. P., Basak, R. K., Basu Majumder, S., & Adhikari, B.

163 (2012). Improvement in mechanical properties of jute fibres through mild alkali  
164 treatment as demonstrated by utilisation of the Weibull distribution model. *Bioresource*  
165 *Technology*, 107, 222–228. <https://doi.org/10.1016/j.biortech.2011.11.073>

166 Saadaoui, N., Rouilly, A., Fares, K., & Rigal, L. (2013). Characterization of date palm  
167 lignocellulosic by-products and self-bonded composite materials obtained thereof.  
168 *Materials and Design*, 50, 302–308. <https://doi.org/10.1016/j.matdes.2013.03.011>

169 Saravanakumar, S. S., Kumaravel, A., Nagarajan, T., & Moorthy, I. G. (2014). Effect of  
170 Chemical Treatments on Physicochemical Properties of Prosopis juliflora Fibers.  
171 *International Journal of Polymer Analysis and Characterization*, 19(5), 383–390.  
172 <https://doi.org/10.1080/1023666X.2014.903585>

173 Saravanakumar, S. S., Kumaravel, A., Nagarajan, T., Sudhakar, P., & Baskaran, R. (2013).  
174 Characterization of a novel natural cellulosic fiber from Prosopis juliflora bark.  
175 *Carbohydrate Polymers*, 92(2), 1928–1933.  
176 <https://doi.org/10.1016/j.carbpol.2012.11.064>

177 Segal, L., Creely, J. J., Martin, A. E., & Conrad, C. M. (1959). An Empirical Method for  
178 Estimating the Degree of Crystallinity of Native Cellulose Using the X-Ray  
179 Diffractometer. *Textile Research Journal*, 29(10), 786–794.  
180 <https://doi.org/10.1177/004051755902901003>

181 Wei, J., & Meyer, C. (2015). Degradation mechanisms of natural fiber in the matrix of  
182 cement composites. *Cement and Concrete Research*, 73, 1–16.  
183 <https://doi.org/10.1016/j.cemconres.2015.02.019>

184